URSI GASS 2021, Rome, Italy, 28 August - 4 September 2021

Hybridized Contrast Source Inversion Method

Serhat Dinleyen* and Hüseyin Arda Ülkü
Department of Electronics Engineering
Gebze Technical University
41400 Kocaeli, Turkey

Abstract

A contrast source inversion based method, which hybridizes the cross-correlated contrast source inversion method (CC-CSIM) and multiplicative regularized contrast source inversion method (MR-CSIM) by applying them consecutively, is proposed for the solution of inverse scattering problems. The proposed method, called hybridized contrast source inversion method (H-CSIM), benefits the effective properties of MR-CSIM and CC-CSIM. A numerical example that demonstrates the robustness to noise, improved reconstruction accuracy, and convergence properties of the proposed method is presented.

1 Introduction

Contrast source inversion method (CSIM) is one of the well-known methods for the solution of the inverse scattering problems [1–11], since CSIM has several benefits, e.g. it does not require the full solution of the forward problem and its computational burden is lower [1–4]. In CSIM, the inverse problem is formulated as an optimization problem with a cost function, which consists of the state and data errors, and then iteratively solved using the conjugate gradient method. In [1], total variation factor is introduced into the cost function of CSIM as a constraint. This method is called multiplicative regularized CSIM (MR-CSIM) and has edge-preserving property compared to CSIM. However the reconstructions might not be stable and/or might not converges to the actual solution for the problems involving high contrast scatterers and/or noisy data. Similar to MR-CSIM, a new error term, which correlates the state and data errors in the measurement domain, is added to the cost function of CSIM to improve the robustness for the problems involving high contrast scatterers and/or noisy data. This method is called cross-correlated CSIM (CC-CSIM) [6, 7].

In this work, hybridization of CC-CSIM and MR-CSIM by applying them consecutively is proposed for the solution of the inverse scattering problems. The proposed method is called hybridized CSIM (H-CSIM). In the proposed method, the reconstruction starts using CC-CSIM to provide robustness to noise and to approach to the global minimum, then at a certain iteration it is switched to MR-CSIM to take advantage of its edge-preserving and converging properties. To demonstrate the effectiveness of H-CSIM, the "Austria" profile [5,6] is analyzed as a numerical example using H-CSIM, MR-CSIM, and CC-CSIM for 2-D TM_z electromagnetic case.

2 Formulation

Let D denote the region of interest, where a non-magnetic unknown scatterer is embedded, and S denote the background medium with the permittivity ε_0 and permeability μ_0, as shown in Figure 1. The receivers and transmitters are located to $\mathbf{r}_m \in S$ and $\mathbf{r}_{\tilde{m}} \in S$, respectively, and $\mathbf{r} \in D$ denotes the position vector. Permittivity of the unknown scatterer is $\varepsilon(\mathbf{r}) = \varepsilon_r(\mathbf{r})\varepsilon_0$, where $\varepsilon_r(\mathbf{r})$ is the complex relative permittivity.

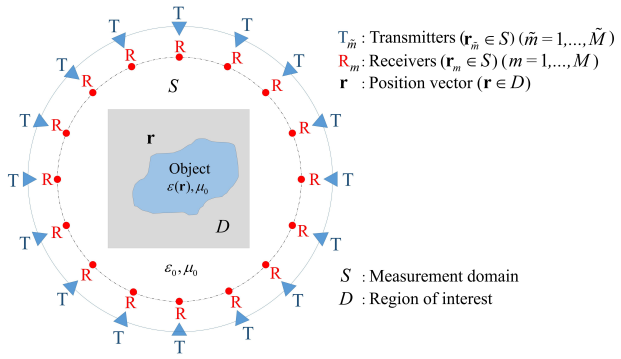

Figure 1. Representation of the inverse scattering problem.

The state and data equations in terms of the z-component of the total electric field $E_z(\mathbf{r})$ and the scattered electric field $E_z^{\mathrm{scat}}(\mathbf{r})$ are given as

$$E_z(\mathbf{r}) = E_z^{\mathrm{inc}}(\mathbf{r}) - k_b^2 \int_D G(\mathbf{r},\mathbf{r}')\chi(\mathbf{r}')E_z(\mathbf{r}')d\mathbf{r}', \mathbf{r} \in D, \quad (1)$$

$$E_z^{\mathrm{scat}}(\mathbf{r}_m) = -k_b^2 \int_D G(\mathbf{r}_m,\mathbf{r}')\chi(\mathbf{r}')E_z(\mathbf{r}')d\mathbf{r}', \mathbf{r}_m \in S, \quad (2)$$

respectively. In (1) and (2), $E_z^{\mathrm{inc}}(\mathbf{r})$ is the incident electric field, $G(\mathbf{r},\mathbf{r}')$ is the Green function of the 2-D homo-

geneous medium, $k_b = \omega\sqrt{\varepsilon_0\mu_0}$ is the wave number of the background medium S, and $\chi(\mathbf{r}) = \varepsilon_r(\mathbf{r}) - 1$ is the contrast.

In CSIM, the contrast and contrast source are updated iteratively by minimizing the cost function that consists of the data and state errors [1]. The contrast source is defined as

$$w_j(\mathbf{r}) = \chi(\mathbf{r})E_{z,j}(\mathbf{r}),\ \mathbf{r} \in D, \tag{3}$$

where "j" denotes the number of sources and/or incident fields. The data and state equations are symbolically given by

$$f_j(\mathbf{r}) = G_S(\mathbf{r},\mathbf{r}')w_j(\mathbf{r}'), \quad \mathbf{r} \in S,\ \mathbf{r}' \in D, \tag{4}$$

$$w_j(\mathbf{r}) = \chi(\mathbf{r})E^{\text{inc}}_{z,j}(\mathbf{r}) + \chi(\mathbf{r})G_D(\mathbf{r},\mathbf{r}')w_j(\mathbf{r}'),\ \mathbf{r},\mathbf{r}' \in D. \tag{5}$$

Here $f_j(\mathbf{r})$ denotes the measured data due to jth source, G_S and G_D are mapping operators described in [1]. Note that for simplicity dependencies of the variables to the position vector will not be shown after this point. The cost function at the nth iteration is defined as

$$F^{\text{CSIM}}_n(w_{j,n},\chi_n) = F_S(w_{j,n}) + F_{D,n}(w_{j,n},\chi_n), \tag{6}$$

where the data and state errors are written as

$$F_S(w_{j,n}) = \eta_S \sum\nolimits_j \left\| f_j - G_S w_{j,n} \right\|^2_S, \tag{7}$$

$$F_{D,n}(w_{j,n},\chi_n) = \eta_{D,n} \sum\nolimits_j \left\| \chi_n E^{\text{inc}}_{z,j} - w_{j,n} + \chi_n G_D w_{j,n} \right\|^2_D, \tag{8}$$

respectively. In (7) and (8), $\|\,.\,\|_D$ and $\|\,.\,\|_S$ operators are L_2 norms on D and S, respectively. Normalization factors are defined as

$$\eta_S = \left(\sum\nolimits_j \left\| f_j \right\|^2_S \right)^{-1}, \tag{9}$$

$$\eta_{D,n} = \left(\sum\nolimits_j \left\| \chi_{n-1} E^{\text{inc}}_{z,j} \right\|^2_D \right)^{-1}. \tag{10}$$

In MR-CSIM [5], the cost function of CSIM given in (6) is multiplied by the weighted L_2 norm of total variation factor:

$$F^{\text{MR-CSIM}}_n(w_{j,n},\chi_n) = F^{\text{CSIM}}_n(w_{j,n},\chi_n) \times F^R_n(\chi_n), \tag{11}$$

where regularization factor $F^R_n(\chi_n)$ is defined as

$$F^R_n(\chi_n) = \frac{1}{V} \int_D \frac{|\nabla\chi(\mathbf{r})|^2 + \delta^2_{n-1}}{|\nabla\chi_{n-1}(\mathbf{r})|^2 + \delta^2_{n-1}} d\mathbf{r}. \tag{12}$$

In (12), V denotes the area of the investigation domain D and δ^2_{n-1} is introduced for restoring the differentiability of the total variation factor [5].

In CC-CSIM [6], an error term, which cross-correlates the data and state errors in the measurement domain, is added to the cost function of CSIM given in (6):

$$F^{\text{CC-CSIM}}_n(w_{j,n},\chi_n) = F^{\text{CSIM}}_n(w_{j,n},\chi_n) + \eta_S \sum\nolimits_j \left\| \xi_{j,n}(w_{j,n},\chi_n) \right\|^2_S, \tag{13}$$

where $\xi_{j,n}(w_{j,n},\chi_n)$ is related to the cross-correlation of the data and state equations and defined as

$$\xi_{j,n}(w_{j,n},\chi_n) = f_j - G_S(\chi_n E^{\text{inc}}_{z,j} + \chi_n G_D w_{j,n}). \tag{14}$$

Detailed information about CSIM, MR-CSIM, and CC-CSIM is available in [1–7].

In hybridized CSIM (H-CSIM), the iterative reconstruction is started using CC-CSIM, because MR-CSIM might not converges to the global minimum and fails to recover the original profile for high contrast scatterers and noisy data compared to CC-CSIM and CSIM as emphasized in [6]. Starting the reconstruction with CC-CSIM ensures the stability and a solution close to the global minimum can be obtained. However as it can be seen in [6], after a certain iteration, the solution obtained using CC-CSIM converges and the reconstruction error saturates, in addition the sharp edges of the scatterers cannot be reconstructed. As a result, at a convenient iteration, called switching iteration (si), the iterative reconstruction is switched to MR-CSIM using the solution at the switching iteration obtained by CC-CSIM as an initial guess. Note that it is also pointed out in [6] that a good initial guess is very important for MR-CSIM, in this case the solution obtained using CC-CSIM provides an initial guess close to the global minimum. Switching to MR-CSIM from CC-CSIM improves the reconstruction accuracy, reduces the reconstruction error, and provides edge-preserving property, especially for the problems involving high contrast scatterers and noisy data.

3 A Numerical Example

In this section, the "Austria" profile is analyzed for 2-D TM_z electromagnetic case and the results obtained for different permittivity values using H-CSIM, CC-CSIM, and MR-CSIM are compared.

The Austria profile has two disks and one ring. The center of the two disks with a radius of 0.2 m are located at $(0.3, 0.6)$ m and $(-0.3, 0.6)$ m. The center of the ring, which has an inner radius of 0.3 m and an exterior radius of 0.6 m, is located at $(0, -0.2)$ m. The complex relative permittivities of the Austria profile are chosen as $\varepsilon_r = \varepsilon'_r - \text{j}\varepsilon''_r = \{2.0 - 0.6\text{j}, 2.5 - 0.6\text{j}, 3.0 - 0.6\text{j}, 3.5 - 0.6\text{j}\}$ [6], where "j" is the imaginary unit.

Synthetic data is generated by solving forward scattering problem using method of moments (MoM) for 36 isotropic line sources and receivers located on a circle centered at $(0, 0)$ with the radius of 3 m at operating frequency 300 MHz. Size of the discretization for the forward problem is chosen between 0.033λ to 0.05λ depending on the permittivity of the Austria profile, where λ is the wavelength in S. Once the forward problem is solved, 10% random additive white noise is added to the solution as explained in [5].

For the inverse problem the discretization size is selected specifically different than the forward problem between

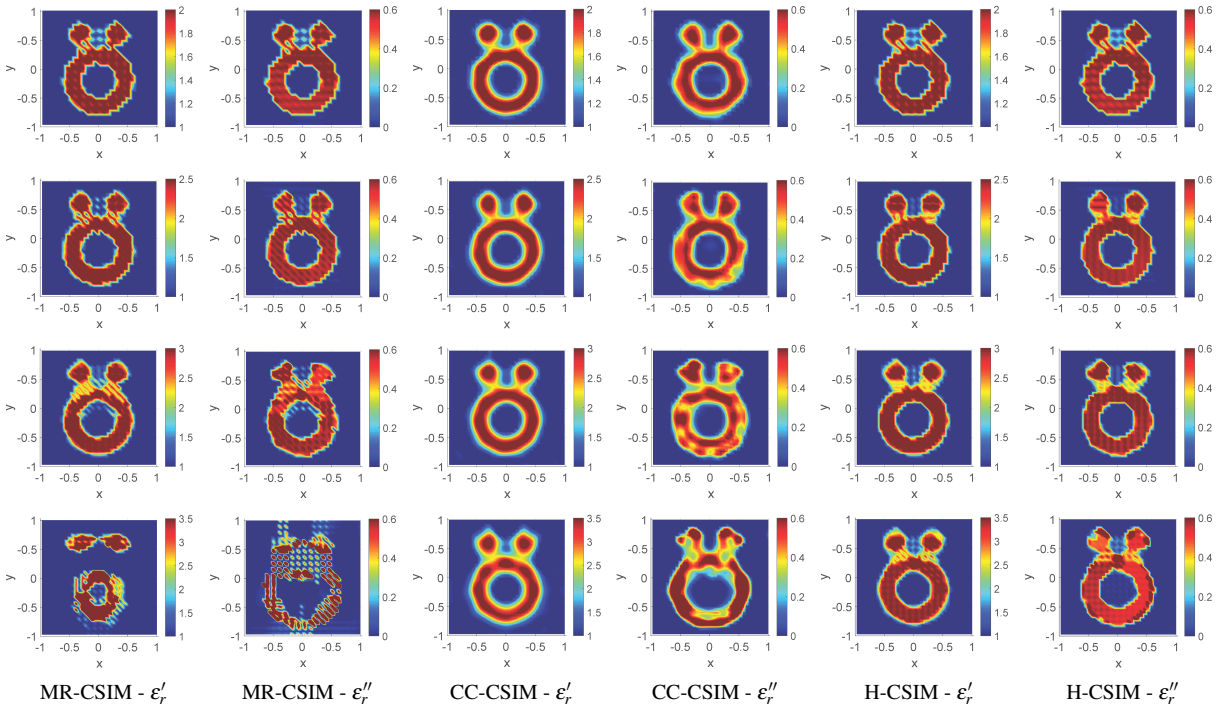

Figure 2. Reconstructed relative permittivity at 2500th iteration for 10% random additive white noise. From left to right: MR-CSIM, CC-CSIM, and H-CSIM with respect to real and imaginary parts of the relative permittivity. From top to bottom: $\varepsilon_r = 2.0 - \mathrm{j}0.6$, $\varepsilon_r = 2.5 - \mathrm{j}0.6$, $\varepsilon_r = 3.0 - \mathrm{j}0.6$, and $\varepsilon_r = 3.5 - \mathrm{j}0.6$. The switching iteration is $\mathrm{si} = 500$.

0.0577λ to 0.0707λ. For all the methods applied in this section, positivity constraint [1] is imposed after each update of the contrast. Initial values of the contrast and contrast source for CC-CSIM are obtained using back propagation as explained in [1]. In H-CSIM, the switching iteration is selected as $\mathrm{si} = 500$ based on the comparison given in [6].

The reconstruction error with respect to iteration number is calculated as

$$Err_n = \frac{\left\| \varepsilon_r - \varepsilon_r^{(n)} \right\|_2^2}{\|\varepsilon\|_2^2}, \qquad (15)$$

where ε_r is the true complex relative permittivity and $\varepsilon_r^{(n)}$ is the reconstructed relative permittivity at nth iteration.

Figure 2 shows the real and imaginary parts of the reconstructed relative permittivities obtained using MR-CSIM, CC-CSIM, and H-CSIM after 2500 iterations for the data disturbed by 10% random additive white noise. Figure 3 plots the associated reconstruction errors. It can be seen from Figures 2 and 3 that MR-CSIM fails to recover the original profile with the increase in relative permittivity, CC-CSIM cannot determine the edges of the Austria profile for almost all cases, whereas H-CSIM has detected the edges more distinctive between the ring and disks. The improved accuracy of the reconstruction for H-CSIM can be also seen in Figure 3, where the effect of the switching from CC-CSIM to MR-CSIM can be clearly seen.

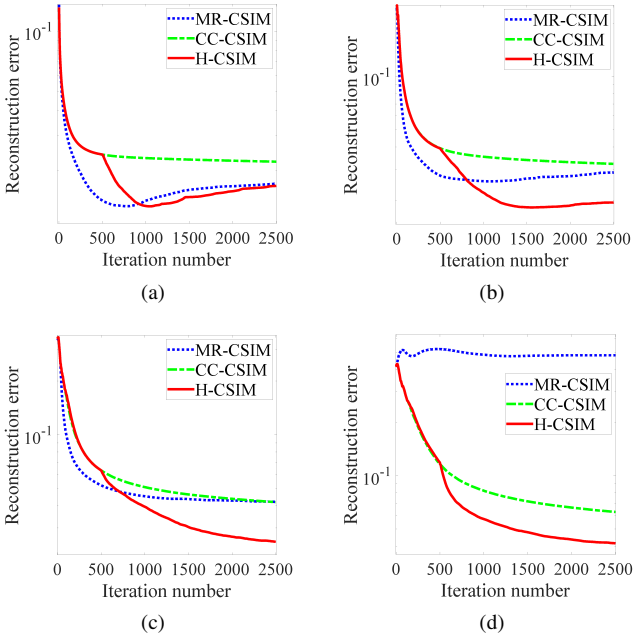

Figure 3. Reconstruction error for disturbed data by 10% random additive white noise: (a) $\varepsilon_r = 2.0 - \mathrm{j}0.6$, (b) $\varepsilon_r = 2.5 - \mathrm{j}0.6$, (c) $\varepsilon_r = 3.0 - \mathrm{j}0.6$, (d) $\varepsilon_r = 3.5 - \mathrm{j}0.6$.

4 Conclusions

Hybridization of the CC-CSIM and MR-CSIM, called hybridized CSIM (H-CSIM), is proposed in this work. The

proposed method is applied to the solution of 2-D TM_z electromagnetic inverse scattering problem and it is shown that H-CSIM has edge-preserving feature compared to CC-CSIM, is more robust to noise compared to MR-CSIM, and provides accurate reconstruction compared to both MR-CSIM and CC-CSIM, especially for the problems involving high contrast scatterers and noisy data.

References

[1] P. Berg and A. Abubakar, "Contrast source inversion method: State of art," *J. Electromagn. Waves Appl.*, vol. 15, no. 11, pp. 1503–1505, Jan. 2001.

[2] K. F. I. Haak, P. M. van den Berg, and R. E. Kleinman, "Contrast source inversion method using multi-frequency data," in *IEEE Antennas Propag. Soc. Int. Symp.*, vol. 2, pp. 710–713, June 1998.

[3] P. Berg, A. Broekhoven, and A. Abubakar, "Extended contrast source inversion," *Inverse Probl.*, vol. 15, no. 5, pp. 1325–1344, Oct. 1999.

[4] A. Abubakar, W. Hu, P. Berg, and T. Habashy, "A finite-difference contrast source inversion method," *Inverse Probl.*, vol. 24, no. 6, pp. 1–17, Sep. 2008.

[5] P. Berg, A. Abubakar, and J. Fokkema, "Multiplicative regularization for contrast profile inversion," *Radio Sci.*, vol. 38, no. 2, pp. 23–1–23–10, Apr. 2003.

[6] S. Sun, B. J. Kooij, T. Jin, and A. G. Yarovoy, "Cross-correlated contrast source inversion," *IEEE Trans. Antennas Propag.*, vol. 65, no. 5, pp. 2592–2603, May 2017.

[7] S. Sun, B. Kooij, and A. Yarovoy, "Inversion of multifrequency data with the cross-correlated contrast source inversion method," *Radio Sci.*, vol. 53, no. 6, pp. 710–723, May 2018.

[8] X. Song, M. Li, F. Yang, S. Xu, and A. Abubakar, "Three-dimensional joint inversion of EM and acoustic data based on contrast source inversion," *IEEE J. Multiscale Multiphys. Comput. Tech.*, vol. 5, pp. 28–36, 2020.

[9] A. Desmal and H. Bagci, "Sparse contrast-source inversion using linear-shrinkage-enhanced inexact Newton method," in *IEEE Antennas Propag. Soc. Int. Symp.*, pp. 870–871, 2014.

[10] C. Gilmore, P. Mojabi, and J. LoVetri, "Comparison of an enhanced distorted Born iterative method and the multiplicative-regularized contrast source inversion method," *IEEE Trans. Antennas Propag.*, vol. 57, no. 8, pp. 2341–2351, Aug. 2009.

[11] A. Zakaria and J. LoVetri, "Application of multiplicative regularization to the finite-element contrast source inversion method," *IEEE Trans. Antennas Propag.*, vol. 59, no. 9, pp. 3495 – 3498, Oct. 2011.